Research Article

Holocene water levels of Silver Lake, Montana, and the hydroclimate history of the Inland Northwest

Meredith C. Parish[a]* 🔵 , Kyra D. Wolf[b], Philip E. Higuera[b] and Bryan N. Shuman[c]

[a]Department of Earth, Environmental, and Planetary Sciences, Brown University, 324 Brook St., Providence, RI 02912, USA; [b]Department of Ecosystem and Conservation Sciences, University of Montana, 32 Campus Drive, Missoula, MT 59812, USA and [c]Department of Geology and Geophysics, University of Wyoming, 1000 E. University Ave., Laramie, WY 82072, USA

Abstract

The wettest portion of the interior of western North America centers on the mountainous region spanning western Montana, Idaho, British Columbia, and Alberta. Inland ranges there capture the remnants of Pacific storms. Steep east–west hydroclimate gradients make the region sensitive to changes in inland-penetrating moisture that may have varied greatly during the Holocene. To investigate potential hydroclimate change, we produced a 7600-yr lake-level reconstruction from Silver Lake, located on the Montana–Idaho border. Ground-penetrating radar profiles and a transect of four shallow-water sediment cores that were dated using radiocarbon dating and tephrachronology revealed substantial changes in moisture through time. An organic-rich mud unit indicating wet and similar to modern conditions prior to 7000 cal yr BP is overlain by an erosional surface signifying drier than modern conditions from 7000–2800 cal yr BP. A subsequent time-transgressive increase in water levels from 2800–2300 cal yr BP is indicated by a layer of late Holocene muds, and is consistent with glacier expansion and increases in the abundance of mesic tree taxa in the region. Millennial-scale trends were likely driven by variations in orbital-scale forcing during the Holocene, but the regional outcomes probably depended upon factors such as the strength of the Aleutian Low, Pacific sea-surface temperature variability, and the frequency of atmospheric rivers over western North America.

Keywords: Paleoclimate, Hydroclimate, Lake level, Holocene, Inland Northwest, Pacific Northwest, Montana

(Received 21 September 2021; accepted 16 March 2022)

INTRODUCTION

Precipitation in western North America falls most heavily along a coastal region extending from northern California to southern Alaska, but coastal mountain ranges and waves in the westerlies limit the inland propagation of this moisture (Rutz et al., 2015). The greatest amount of inland precipitation falls in the northern Rocky Mountains between Idaho and Alberta (Fig. 1; Kalnay et al., 1996), where wet, temperate conditions support a greater diversity of tree populations (Gavin, 2009), a larger network of mountain glaciers (Krimmel, 2002), and higher river runoff than in drier mountain chains to the south and east (Livneh et al., 2013). However, the wet climate of these inland areas may have been susceptible to change during the Holocene (Hermann et al., 2018), especially when considering present-day effects of interannual variability.

Historically, snowpack in the Inland Northwest of the USA (eastern Washington and Oregon, Idaho, and Montana) depends on the strength of the Aleutian Low and associated high-pressure ridging downstream over western North America (Cayan, 1996; Pederson et al., 2011a). Periods of anomalously low pressure in the North Pacific near the Aleutian Islands and anomalously high pressure ridging over western North America coincide with decreased winter

precipitation in the Pacific Northwest and northern Rocky Mountains (Cayan, 1996; Pederson et al., 2011a), including in northwestern Montana (Schoenemann et al., 2020). During the past 800 years, tree-ring-based snowpack reconstructions reveal a north–south anti-phasing of snowpack anomalies in the Rocky Mountains, implicating decadal-scale latitudinal shifts of winter storm tracks thought to be determined by these pressure systems (Pederson et al., 2011b). North Pacific sea-surface temperatures (SSTs) control the modes of atmospheric circulation and the strength and latitudinal position of winter storm tracks (Pederson et al., 2011b). Additionally, a warm North Pacific can increase atmospheric water vapor and thus influence the delivery of moisture to North America during atmospheric river events. These events can change in intensity, frequency, and/or location, and contribute ~35% of the annual precipitation in the inland mountains of western Montana (Gershunov et al., 2017).

Evidence for large changes in the hydroclimatological regime in the Inland Northwest consists of late Holocene forest changes, including the expansion of disjunct populations of western hemlock (*Tsuga heterophylla*) and mountain hemlock (*T. mertensiana*) in the interior mountains from Idaho to northern British Columbia (Gavin, 2009; Herring et al., 2017); evidence of glacier expansion (Menounos et al., 2009; Larsen et al., 2020; Chellman et al., 2021); lake formation (Schweger and Hickman, 1989; Liefert and Shuman, 2020); and lake-level changes (Stone and Fritz, 2006; Shuman et al., 2009; Galloway et al., 2011). Most
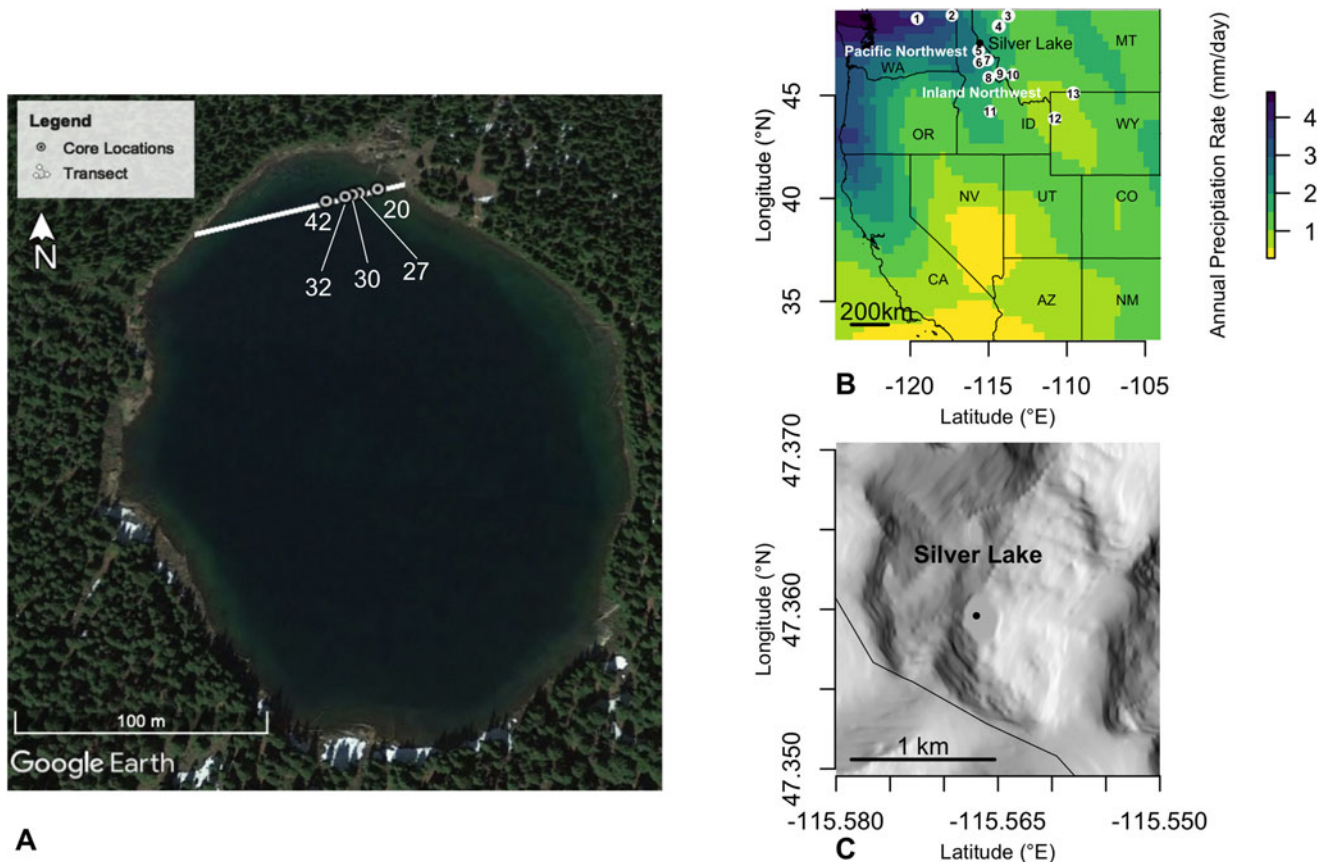
Figure 1. Location maps of study area. (A) Photo of Silver Lake, showing where five cores were taken in a transect at the north end of Silver Lake where there is a small outlet stream (Google Earth Pro, 2021). Cores 20, 27, 30, 32, and 42 were labeled to indicate distance from lake shore in meters. (B) Map of the western United States showing annual precipitation rate in mm/day. Note that average precipitation rate from 1981–2010 in the Bitterroot Mountains of the Northern Rocky Mountains where Silver Lake is located was about 2.5 mm per day (Kalnay et al., 1996). Locations of other published hydroclimate proxy records along the northern Rocky Mountains are: 1) Castor Lake, 2) Lime Lake, 3) Hidden Lake, 4) Foy Lake, 5) Dismal Lake, 6) Rocky Ridge Lake, 7) Horseshoe Lake, 8) Burnt Knob Lake, 9) Baker Lake, 10) Pintlar Lake, 11) Lower Decker Lake, 12) Delta Lake, 13) Beartooth Ice Patch. (C) Shaded elevation map of Silver Lake (USGS, 2017), a small cirque lake in a small watershed on the Idaho–Montana border, plotted using the R package raster (Hijmans et al., 2022).

proxy records in the northern Rocky Mountains indicate a mid-to late Holocene increase in moisture (Hermann et al., 2018; Liefert and Shuman, 2020), continuing an increase in annual moisture driven by long-term changes in insolation and greenhouse gas concentrations during the Holocene (Bartlein et al., 1998; Kutzbach et al., 1998; Diffenbaugh et al., 2006; Routson et al., 2019). However, northern Washington and British Columbia appear to have experienced declining moisture (Galloway et al., 2011; Steinman et al., 2019), calling in to question the ubiquity of broader regional trends in moisture at sites in the Inland Northwest.

Here, we evaluate how the hydroclimate of the Inland Northwest has varied over the past 7600 years in response to late Holocene warming in the northeastern Pacific (Barron et al., 2003), the strengthening of the Aleutian Low (Barron and Anderson, 2011), possible decreases in upper-level ridging off the coast of the Pacific Northwest (Hermann et al., 2018), potential reductions in atmospheric river frequency in the Pacific Northwest (Skinner et al., 2020), and the increasing equator-to-pole temperature gradient (Routson et al., 2019). We focus on the water-level history of Silver Lake, Montana in the northern Bitterroot Mountains along the Montana–Idaho border to examine the hydrologic history of high elevations in Idaho and northwest Montana that are most affected at present by inland

penetration of atmospheric rivers (Rutz et al., 2014). The site lies 130 km southwest of Foy Lake, which has had a previous lake-level reconstruction produced (Shuman et al., 2009), and is situated near the locations of several paleoecological studies (Whitlock and Bartlein, 1993; Brunelle et al., 2005, 2008; Stone and Fritz, 2006; Power et al., 2006, 2011; Whitlock et al., 2008; Herring and Gavin, 2015; Herring et al., 2017). To reconstruct hydroclimatic changes at Silver Lake during the Holocene, we conducted geophysical surveys, and collected sediment cores across a transect encompassing a range of water depths to identify past changes in shoreline position. The lake-level reconstruction adds to the spatial coverage of paleohydrology records from the Inland Northwest, allowing us to evaluate potential Holocene climate forcings on the Inland Northwest hydroclimate.

STUDY SITE

Silver Lake (47.3596°N, 115.565912°W, 1623 m asl 5.26 ha area) occupies a basin along the ridgeline of the Montana–Idaho border in the northern Bitterroot Mountains southwest of Lookout Pass (Fig. 1). The lake lies in a Late Pleistocene cirque and is dammed by a glacial moraine (Locke, 1990). Silver Lake has a maximum depth of 18.8 m, an ~100-ha watershed with no significant input streams, and a seasonal outlet stream on the north side of
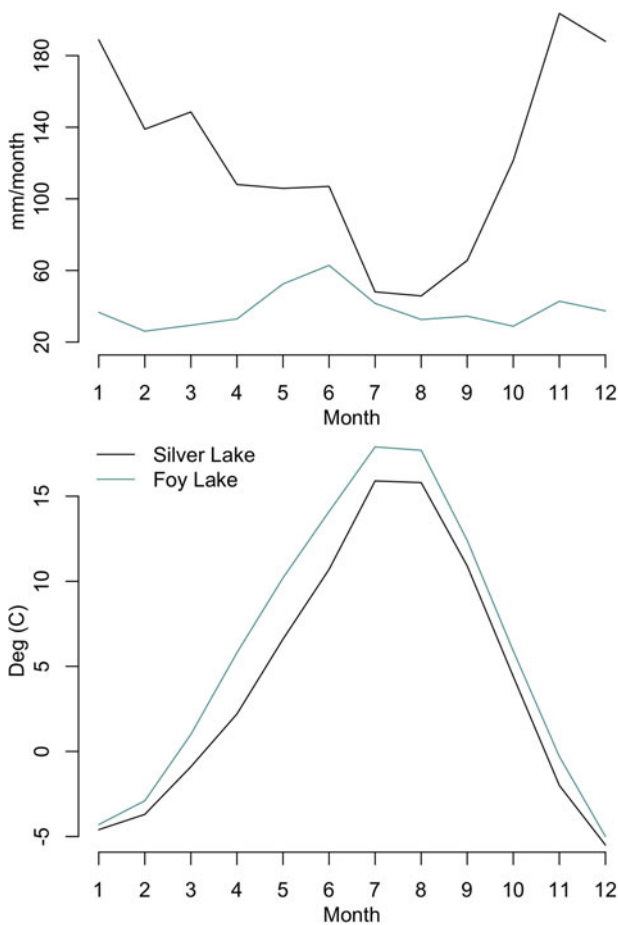
Figure 2. Graphs comparing PRISM 800-m resolution, 30-year precipitation (upper) and temperature (lower) normals (1981–2010) for Silver Lake and Foy Lake (PRISM Climate Group, 2021).

et al., 2015), and marks the easternmost latitude experiencing a surplus of January moisture, characteristic of the Pacific Northwest, as indicated by high values of actual evaporation/potential evaporation (AE/PE; Shinker and Bartlein, 2010). Around Silver Lake, AE/PE values are ~0.8 from October–May, and drop to ~0.4 in July and August, indicating late summer evaporative stress (Shinker and Bartlein, 2010).

METHODS

Fieldwork

We used a Geophysical Survey Systems, Inc. SIR-3000 ground-penetrating radar (GPR) with 400-MHz antennae in 2017 to evaluate the location of paleoshorelines that appear as reflectors beneath the lake sediment surface. Based on the GPR surveys, we selected a coring transect perpendicular to shoreline to capture a continuous stratigraphic sequence of paleoshoreline changes as demonstrated in previous studies (Shuman, 2003; Newby et al., 2014; Shuman et al., 2015). A transect of sediment cores was collected at Silver Lake between 20 m to 42 m from shore in water depths ranging from 2.3 m to 3.3 m. The cores were taken in the shallow bay near the lake outlet and labeled to indicate lateral distance from the shore. The cores were targeted to capture paleoshoreline deposits and erosional features associated with reflectors in the GPR images (Digerfeldt, 1986; Harrison and Digerfeldt, 1993; Pribyl and Shuman, 2014). Cores were recovered by hand with a 7-cm-diameter piston corer using polycarbonate tubing lowered from a raft along the transect.

Core analyses

At the University of Wyoming, we logged the cores using a Geotek, Ltd. Multi-Sensor Core Logger in our lab to obtain gamma-attenuation bulk density and magnetic susceptibility, then subsampled the cores at 1-cm contiguous intervals to measure sand and organic content. Sand and organic content can differentiate sediments that accumulated in the high-energy depositional environments of shallow shoreline areas from deep-water organic muds that accumulated offshore in still water below the thermocline (Digerfeldt, 1986; Rowan et al., 1992; Harrison and Digerfeldt, 1993). We wet-sieved the samples using 63-μm mesh to measure sand content, and performed loss-on-ignition analyses using standard techniques to estimate sediment organic content (Shuman, 2003).

To determine the timing of facies changes at Silver Lake, we obtained radiocarbon dates on sedimentary charcoal and plant macrofossils (conifer needles) from the cores. We picked charcoal and macrofossils for radiocarbon analyses from core intervals that bracketed sand layers (inferred to be paleoshoreline deposits) after wet-sieving 1-cm-thick subsamples using a 125-μm mesh. Because the materials were picked from organic-rich profundal mud intervals, they were not significantly affected by lake mixing or sediment reworking. Samples were analyzed at the Keck Carbon AMS Laboratory at the University of California, Irvine. We calibrated the radiocarbon ages to calendar years using IntCal20 (Reimer et al., 2020) with the R Package Bchron (Parnell, 2021). The ages are presented as calibrated years before AD 1950 (hereafter, cal yr BP). In addition to radiocarbon dates, we used visual inspection and magnetic susceptibility measurements to identify tephra layers within the cores. From our samples, we separated tephras by hand that were then analyzed by

the cirque. Within the lake, a bathymetric shelf located at the mouth of the outflow stream creates a shallow bay that we targeted for our analyses. The high topographic location of the lake limits regional groundwater input. Silver Lake lies on the Proterozoic-aged Wallace Formation, which is dolomitic siltite and quartzite capped by black argillite, and locally is intersected by a diorite and gabbro dike (Lonn and McFaddan, 1999). Glacial tills cover the Wallace Formation meta-sediments, and are vegetated by subalpine forest, including subalpine fir (*Abies lasiocarpa*), Engelmann spruce (*Picea engelmannii*), lodgepole pine (*Pinus contorta*), and mountain hemlock.

The Silver Lake watershed has a winter-dominated precipitation regime with >180 mm of precipitation per month from November through January based on the 1981–2010 climate normals (Fig. 2; PRISM Climate Group, 2021). The watershed receives only ~60 mm of precipitation per month in the driest months of July and August. The winter precipitation regime at Silver Lake contrasts with low-elevation areas to the east, such as Foy Lake, which receives less precipitation, ranging from a low of 20 mm in February to a high of 60 mm in June (Fig. 2). The present climate of Silver Lake places it within the greater Pacific Northwest region, which received over 2.5 mm of precipitation per day on average from 1981 to 2010 (Fig. 1; Kalnay et al., 1996).

Silver Lake lies directly within the region with the greatest frequency of interior-penetrating atmospheric river events (Rutz

an electron microprobe at the Peter Hooper GeoAnalytical Laboratory School at Washington State University. The glass shards from the samples were analyzed to identify % SiO_2, Al_2O_3, Fe_2O_3, TiO_2, Na_2O, K_2O, MgO, CaO, and Cl. The accepted age of identified tephras was assigned to our samples. Bchron was then used to develop age–depth models for each core based on the combination of radiocarbon and tephra ages.

Lake-level reconstruction

We reconstructed the lake-level history at Silver Lake using a decision-tree approach in R to iteratively classify every 1-cm sample from all four cores as littoral, sublittoral, or profundal based on the percentage of sand in each core. Reconstructing multiple iterations of lake-level change using varying facies definitions provides uncertainty estimates around the reconstruction. Samples were classified as shallow littoral sediments when sand content exceeded 15–40%, at 5% intervals. Samples were denoted as representing deep-water conditions when sand content fell below 5–15%, at 1% intervals. Core classification was conducted iteratively based on all possible combinations of the two thresholds. For each iteration, we used the resulting classification of each sample in each core, the age-depth models, and the depth of each sample below the modern water level to reconstruct the elevation of the littoral-profundal boundary through time; the final reconstruction represents the median and 95% distribution of the different iterations (Pribyl and Shuman, 2014; Shuman and Serravezza, 2017).

RESULTS

GPR surveys

GPR surveys at Silver Lake revealed stratified lacustrine sediments draped across the shallow outlet bay (Fig. 3). Within 10 m of the modern shoreline, the sediment sequence contained a chaotic set of reflectors indicative of piles of woody debris that have accumulated along the lake margin. Farther than 10 m from the shoreline, the sediments were more uniform but one major reflector pair truncated the dipping beds and created a near-shore unconformity consistent with low water (Fig. 3). As illustrated in Figure 3, the reflector pair appeared as two parallel white reflectors extending out from shore, which became faint in the deepest areas. The stratified reflectors at the top of the lake-sediment sequence lapped (intercepted at different points) on to the unconformity between 20 and 30 m from shore (Fig. 3).

Stratigraphy

Cores were collected 42 m, 32 m, 30 m, 27 m, and 20 m from shore to intersect the major reflector and unconformity in the GPR profile (Fig. 3). The cores were collected in 233 cm, 260 cm, 280 cm, 273 cm, and 330 cm of water, respectively (Table 1). Core 20 was not analyzed in detail because radiocarbon dating indicated it only captured the most recent high-water phase of the lake's history (see below). The remaining cores contained a sequence of organic-rich silts, which included several major units (Fig. 4). All cores deeper than core 27 contained basal silts that were ~20–90 cm thick with <20% organic matter; the thickest basal unit was found in core 42, which was the deepest core. Above the basal silts, a sand-rich layer marked the transition to organic-rich muds, which often contained layers of woody debris. A second sand layer was also evident in cores 30 and 32, which likely correlates stratigraphically with the one sand layer at the base of core 27. The muds above the sands varied in organic content, but typically contained ~40% organic matter, except in the debris intervals that reached >60% organic matter, for example, as recorded by peaks in loss-on-ignition in the middle of cores 30 and 32. Two tephra layers, notable as peaks in magnetic susceptibility but also evident upon visually examining all cores, punctuated the uppermost silts in all the cores (Fig. 4). The uppermost silts also are characterized as having a reduced organic content.

The prominent sand layer marked a shift in sediment composition just below 100-cm depth from low to high organic content and high to low magnetic susceptibility in cores 30 and 32. There was also a slight increase in sand content in core 42 at 150-cm depth. Sand content reached >80% in cores 30 and 32, where it was visibly apparent, but only 20% in core 42 (Fig. 4). The second layer of visible sand at 88-cm depth in core 30 and 92-cm depth in core 32 may correspond to the sand layer near the bottom of core 27 that reached 50% sand content. The second sand layer did not extend to core 42, which is consistent with the reflector in the GPR data near core locations 32–27 that truncated the underlying stratigraphy as it merged with the lower paleoshoreline
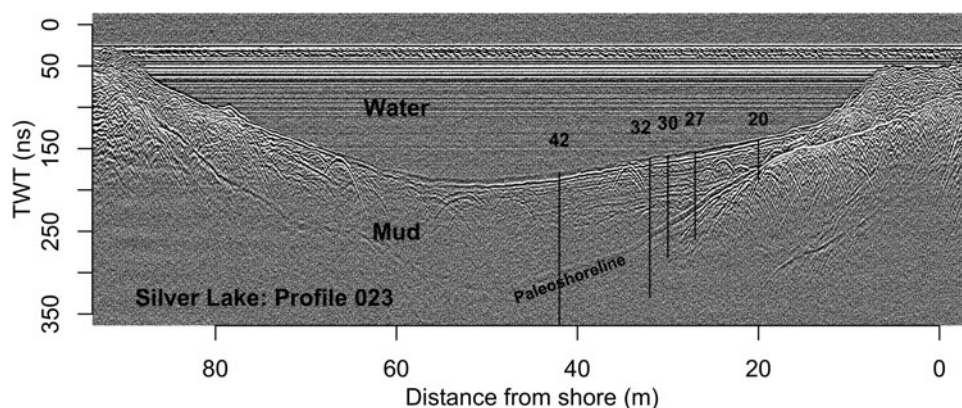

Figure 3. A ground-penetrating radar (GPR) profile from Silver Lake showing the near-shore truncation of sediment layers consistent with past low-water episodes. Vertical scale shows the two-way travel time (TWT) of the radar signal in nanoseconds (ns). Vertical bars show locations of cores 20, 27, 30, 32, and 42 that labeled indicating distance from the lake shore in meters. Sedimentological analyses were performed on cores 42, 32, 30, and 27. A reflective layer below the sediment–water interface indicates a paleoshoreline that interrupts both underlying and upper, onlapping sediment units.

Table 1. Depths and ages from cores 20, 27, 30, 33, and 42 from Silver Lake. Radiocarbon ages are calibrated in IntCal20 (Reimer et al., 2020) with the R Package Bchron (Parnell, 2021).

Core	ID	Core depth (cm)	C^{14} yr BP	Material	Water depth (cm)	Age (cal yr BP)		
						Cal. 05*	Cal. Median**	Cal. 95***
20	UCI-203103	50.5	2360	Charcoal	233	2346	2353	2416
27	–	10	–	1980 MSH Tephra	260	–	−30.00	–
27	–	36	–	MSH J Tephra	260	–	500.00	–
27	UCI-203110	81.5	1870	Charcoal, Needle	260	1732	1776	1819
27	UCI-203109	95.5	2480	Charcoal, Needle	260	2474	2586	2698
27	UCI-203108	100.5	6645	Charcoal, Needle	260	7478	7531	7568
30	–	4	–	1980 MSH Tephra	280	–	−30.00	–
30	–	34	–	MSH J Tephra	280	–	500.00	–
30	UCI-203105	97.5	2550	Charcoal, Needle	280	2547	2720	2736
30	UCI-203106	112.5	6765	Charcoal, Needle	280	7579	7617	7664
30	UCI-203104	125.5	6680	Needle	280	7506	7534	7585
32	SHB1908-1_21_22	11	–	1980 MSH Tephra	273	–	−30.00	–
32	SHB1908-2_23_54	44	–	MSH J Tephra	273	–	500.00	–
32	UCI-203107	104.5	4820	Charcoal, Needle	273	5484	5516	5588
32	UCI-203102	113.5	2750	Needle	273	2787	2823	2871
32	UCI-203111	123.5	6210	Charcoal, Needle	273	7019	7085	7221
32	UCI-203112	157.5	6640	Charcoal, Needle	273	7473	7529	7566
42	–	20	–	1980 MSH Tephra	330	–	−30.00	–
42	–	45	–	MSH J Tephra	330	–	500.00	–
42	UCI-203113	224.5	6325	Needle	330	7173	7207	7295

*Cal. 05 refers to the 5% confidence interval of the age model.
*Cal. median refers to the median calibrated year before AD 1950 (cal yr BP), which was used to plot the data.
*Cal. 95 refers to the 95% confidence interval of the age model.

reflector at ∼ 27–25 m from shore, and disappeared about 35 m from shore (Fig. 3).

Radiocarbon stratigraphy

Ten radiocarbon dates from macrofossils and charcoal resulted in ages younger than 8000 cal yr BP after calibration (Table 1, Fig. 4). Samples taken near the base of the cores dated consistently to 7210–7530 cal yr BP (median ages), except for the basal sample from core 20 that dated to 2350 cal yr BP (Table 1). Samples below the major sand layer in cores 30 and 32 have median ages of 7620 and 7090 cal yr BP, although the former appears out of stratigraphic order. Samples above the sand layer, 10 cm and 15 cm stratigraphically higher in cores 30 and 32, respectively, date to median ages of 2820 and 2720 cal yr BP. Consequently, the accumulation of mud on top of the sand layer in cores 32 and 30 and near the bottom of cores 27 and 20 appeared to follow a time-transgressive sequence from deep to shallow cores at 2820, 2720, 2590, and 2350 cal yr BP (median ages). Ages from core 27 constrained the age of the second sand layer as between 2590 and 1780 cal yr BP.

The net sedimentation rates associated with the sand layers in cores 32 and 30 were also exceptionally low: 2.3–5.8 cm/kyr (Fig. 4). After ca. 2300 cal yr BP, all cores accumulated at rates of 25.4–51.5 cm/kyr, which is consistent with the high rates of accumulation below the sand layers of 28.4–76.5 cm/kyr (Fig. 4).

Two radiocarbon ages, one in core 30 and one in core 32, were not in stratigraphic order and thus not included in the age-depth model. The radiocarbon age from the bottom of core 27 (median age: 7530 cal yr BP) also was not included because it represented a period of near-zero sediment accumulation before ca. 2700 cal yr BP.

Additional age constraints were provided in every core through the identification of the two ash layers of known age (Fig. 4; Table 2). Based on its geochemical composition, the most recent tephra was identified as being from the AD 1980 Mount St. Helens eruption, and the tephra below was identified as being from the Mount St. Helens J eruption at ca. 500 cal yr BP (Table 2). The basal radiocarbon dates from the cores are about
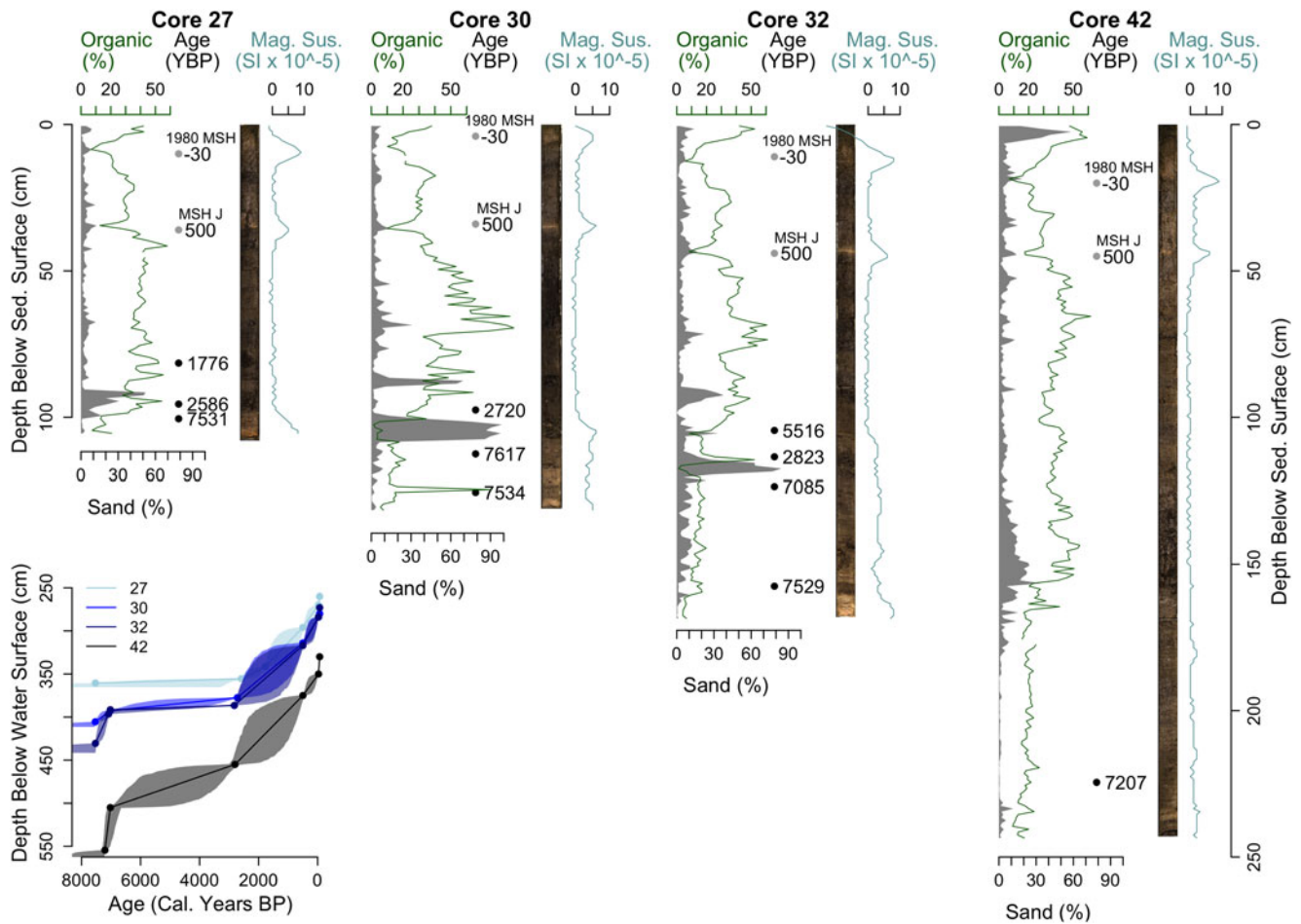
Figure 4. Stratigraphic, sedimentological, chemical, and age data for cores 27, 30, 32, and 42 from Silver Lake include evidence of a low-water phase recorded by high sand content (% inorganic >63 µm shaded in gray), low loss-on-ignition at 550°C (as a measure of sediment organic content, green lines), and changes in magnetic susceptibility (blue lines). Digital photo images show the visual stratigraphy and the age-depth relationships in the cores, including mid-Holocene phases of limited accumulation consistent with shallow water based on calibrated radiocarbon ages (black circles) and tephra ages (gray circles) that are also plotted on bottom left graph, where the shading represents the 95% confidence intervals. MSH is Mount St. Helens.

the age of the Mazama Ash, although we did not conduct a chemical analysis of the basal sediment. Deep-water cores from the center of Silver Lake, not discussed here, penetrate the Mazama Ash to produce a longer record (unpublished data).

Evidence of low-water phases

Qualitative interpretation of the sediment core stratigraphies indicated substantial water-level changes in the past. The combined lines of evidence from continuous GPR reflectors blanketing the lake, sand layers that were traceable across the transect of nearshore cores, and congruent radiocarbon dates confirming low sedimentation rates associated with the sands, indicate a series of water-level changes at Silver Lake. First, a phase of high water (7600–7000 cal yr BP) initiated the accumulation of the basal silts in cores 42, 32, and 30 (Fig. 4). Second, truncated GPR reflectors, sand layers, and low net sedimentation rates between ∼7000 and 2800 cal yr BP indicate a major, mid-Holocene low-water phase. The time-transgressive deposition of organic-rich mud above the sand layer in cores 32, 30, and 27 is consistent with the shoreward onlap of GPR reflectors, and indicates a progressive rise in water level from ca. 2800–2300 cal yr BP. This water-level rise initiated accumulation in cores 27 and 20

after ca. 2500 cal yr BP. The second sand layer present in cores 30 and 32 may indicate an additional low-water phase sometime between ca. 2300–1800 cal yr BP; however, additional radiocarbon dates are needed to verify the timing of this second low-water phase. Finally, after 1800 cal yr BP, the lake likely remained sufficiently high to overflow at least seasonally, as occurs at present.

Quantitative water-level reconstruction

The iterations of lake-level reconstructions with varying thresholds resulted in an ensemble of quantified lake-level histories that are consistent with the qualitative interpretation (Fig. 5). The reconstructed elevation of past water levels indicated changes as great as 300 cm during the past 7600 years. From the beginning of our core record to 7000 cal yr BP, the reconstructed lake level was likely near the modern lake level. The lake then experienced a persistent low phase about 300 cm below the modern lake level from 7000 to 2800 cal yr BP before rising ∼200 cm after ca. 2750 cal yr BP. The second sand layer in cores 27, 30, and 32 may indicate another multi-meter fluctuation at ca. 2300 cal yr BP, but the duration of this low phase is only constrained by two radiocarbon dates. After 1800 cal yr BP, the lake level slowly increased to its modern elevation, which is higher than all

Table 2. Glass composition of tephra layers in weight % oxides normalized to 100%, and probable ages of volcanic eruptions. MSH: Mount St. Helens.

ID	SiO$_2$	Al$_2$O$_3$	Fe$_2$O$_3$	TiO$_2$	Na$_2$O	K$_2$O	MgO	CaO	Cl	Total Shards	Similarity Coefficient	Probable Eruption	Probable Source Age (cal yr BP)
SHB1908-1_21_22	72.03	14.79	2.43	0.34	5.31	2.01	0.59	2.40	0.10	25	0.97	1980 MSH	−30
SHB1908-2_23_54	75.63	13.27	1.61	0.21	4.98	2.53	0.27	1.41	0.09	12	0.97	MSH J	500

previous reconstructed water levels, and consistent with the onset of deposition in cores 27 and 20. Because the lake overflows at its current level, it was not possible to determine whether any periods represented wetter conditions than at present.

DISCUSSION

Comparisons to regional paleoclimate

Paleovegetation records from sites near Silver Lake support the inference of a transition from a dry Mid-Holocene to a wet late Holocene. Mesophilic conifers, such as mountain hemlock and western larch (*Larix occidentalis*), expanded and increased in abundance in the northern Bitterroot Mountains over the late Holocene (Herring et al., 2017). Mountain hemlock appeared 1000 km south of Silver Lake at Horseshoe Lake and Rocky Ridge Lake by 4100 and 1600 cal yr BP, respectively, and was present just 30 km south of Silver Lake at Dismal Lake by 800 cal yr BP (Herring et al., 2017). Before 3300 cal yr BP, Mid-Holocene macrofossils document a drier, less diverse forest than found today at Dismal Lake, dominated by Grand fir (*Abies grandis*) and Douglas fir (*Pseudotsuga menziesii*) (Herring et al., 2017). Likewise, in the southern Bitterroot and adjacent Clearwater ranges, the development of a modern forest composition by 3000 cal yr BP and an increase in arboreal pollen at Burnt Knob, Baker, and Pintlar lakes from the mid- to late Holocene suggests higher moisture in the Late Holocene compared to the mid-Holocene (Brunelle et al., 2005). Farther south at Lower Decker Lake in the Sawtooth Range of central Idaho, pollen evidence of closed-canopy Douglas fir forest was also used to infer the driest period of the Holocene from 5500 to 3380 cal yr BP (Whitlock et al., 2011).

Our lake-level reconstruction is also consistent with the history of Foy Lake, Montana, which has been extensively studied on annual to millennial timescales in the Holocene (Stone and Fritz, 2004, 2006; Stevens et al., 2006; Power et al., 2006, 2011; Shuman et al., 2009; Bracht-Flyr and Fritz, 2012; Schoenemann et al., 2020). Near-shore cores at Foy Lake indicate reduced near-shore sand deposition during a brief high-water phase at ca. 7600 cal yr BP, and a prolonged mid-Holocene low stand represented by high sand deposition (Shuman et al., 2009). Sand deposition in deep areas of the lake is thus recorded at both lakes from ca. 7000–2800 cal yr BP. At Foy Lake, the onset of varve formation over the shallow water sands after ca. 2500 cal yr BP supports the inferred late Holocene increase in effective moisture (Shuman et al., 2009), consistent with the expansion of Silver Lake as marked by the basal age of 2346–2416 cal yr BP in core 20 (Table 1). A benthic diatom record from Foy Lake exhibited a sharp decline in benthic diatom abundance at ca. 2000 YPB, which indicated a deepening of Foy Lake in response to wetter conditions in the late Holocene (Figure 6C; Stone and Fritz, 2006). The gradual decrease in xeric (*Pinus contorta*, *Pinus ponderosa*, *Pseudotsuga*, *Larix*, *Artemisia*, Poaceae, Chenopodiaceae, Cupressaceae) relative to mesic (*Abies*, *Picea*, *Tsuga heterophylla*) pollen taxa measured in a core from the center of Foy Lake from 6000 to 2600 cal yr BP also indicated increasing moisture in the Late Holocene (Fig. 6C; Power et al., 2006, 2011).

An aragonite:calcite record from Jones Lake, located in west-central Montana, also reflects a wet late Holocene with modern, high-moisture conditions established at ca. 1400 cal yr BP (Shapley et al., 2009). Diatom assemblages from elsewhere in Montana suggest similar hydroclimate histories. At Hidden Lake in northwest Montana, the diatom record indicates similar
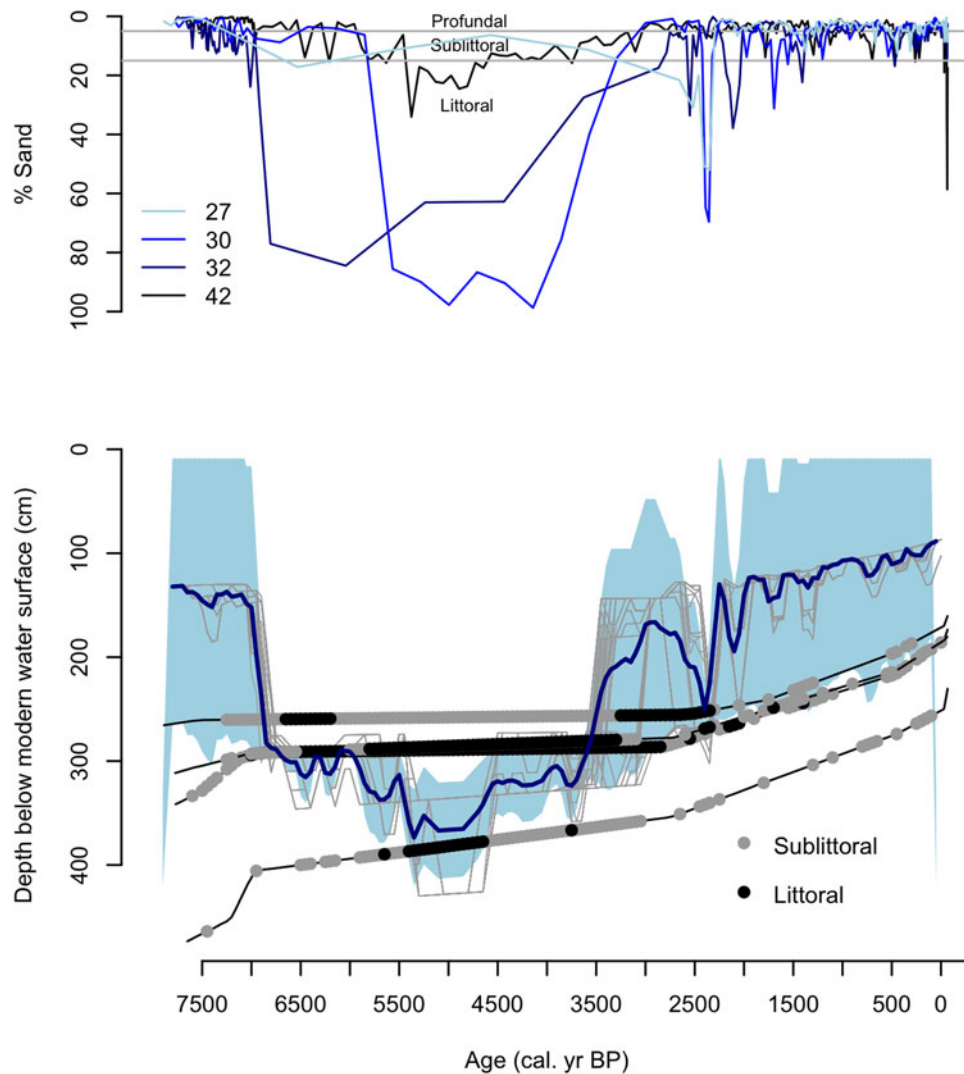
Figure 5. Graphs of % sand and depth below modern water surface versus age for four cores from Silver Lake. Top graph: % sand from cores 27, 30, 32, and 42 plotted versus time with thresholds of % sand used for classifying sediment samples as representing littoral, sublittoral, and profundal environments indicated. Bottom graph: Age-depth relationships: sand data constrain the reconstructed position of the 'sediment limit' (sand–mud boundary) through time based on the elevation of littoral and sublittoral sediments below the modern lake surface (colored circles). The ensemble mean estimate of the sediment limit position, which represents the changing position of the shoreline, is shown as a blue line with light blue shading indicating the range of uncertainty; individual reconstructions in each ensemble shown in gray.

to modern lake levels before 7610 cal yr BP, lower than modern lake levels from 6180 and 4130 cal yr BP, and modern lake levels after 1400 cal yr BP (Stone et al., 2019). Diatom data from Upper Kintla, Beauty, and Emerald lakes elsewhere in the Bitterroot Mountains reveal changes in lake stratification, which can be dependent on the strength of the Aleutian Low, with increased lake mixing when the Aleutian Low weakens and shifts westward (Stone et al., 2016). Stone et al. (2016) inferred decreased storm frequencies across the Pacific Northwest between 4500 and 3300 cal yr BP, increased frequencies between 3200 and 1400 cal yr BP, then a decline from 1300 cal yr BP to present. More work is needed to assess the relationship between the strength of the Aleutian Low and changes in precipitation and the net effective moisture of the region, but changes in the tracks, frequency, or water-vapor content of storms originating from the Pacific Ocean were likely significant influences (Skinner et al., 2020).

Other hydroclimatic reconstructions provide support for broad-scale increases in precipitation from the Mid- to Late Holocene across the Inland Northwest and adjacent regions. Lake-level records spanning the Rocky Mountains from Colorado to Canada reveal increasing water levels over the past 8000 years (Shuman et al., 2009; Shuman and Serravezza, 2017; Liefert and Shuman, 2020). Evidence of glacial advances from Wyoming to Canada also indicate increased precipitation and cooler conditions in the past 3000 years relative to earlier in the Holocene (Fig. 6; Menounos et al., 2009; Larsen et al., 2020; Chellman et al., 2021). For example, increasing rates of ice accumulation at the Beartooth Ice Patch in northwestern Wyoming reflect an increase in precipitation and decrease in temperature after ca. 4000 cal yr BP (Fig. 6A; Chellman et al., 2021). In northwestern Wyoming, increasing input of clastic sediment into Delta Lake indicates expansion of adjacent glaciers starting at ca. 6300 cal yr BP and continuing until 2800 cal yr BP (Fig. 6B; Larsen et al., 2020). A principal component analysis performed on loss-on-ignition data from Green, lower Joffre, Diamond, and Red Barrel lakes in western Canada was also used to infer glacial advances since 8500 cal yr BP (Fig. 6B; Menounos et al., 2009).
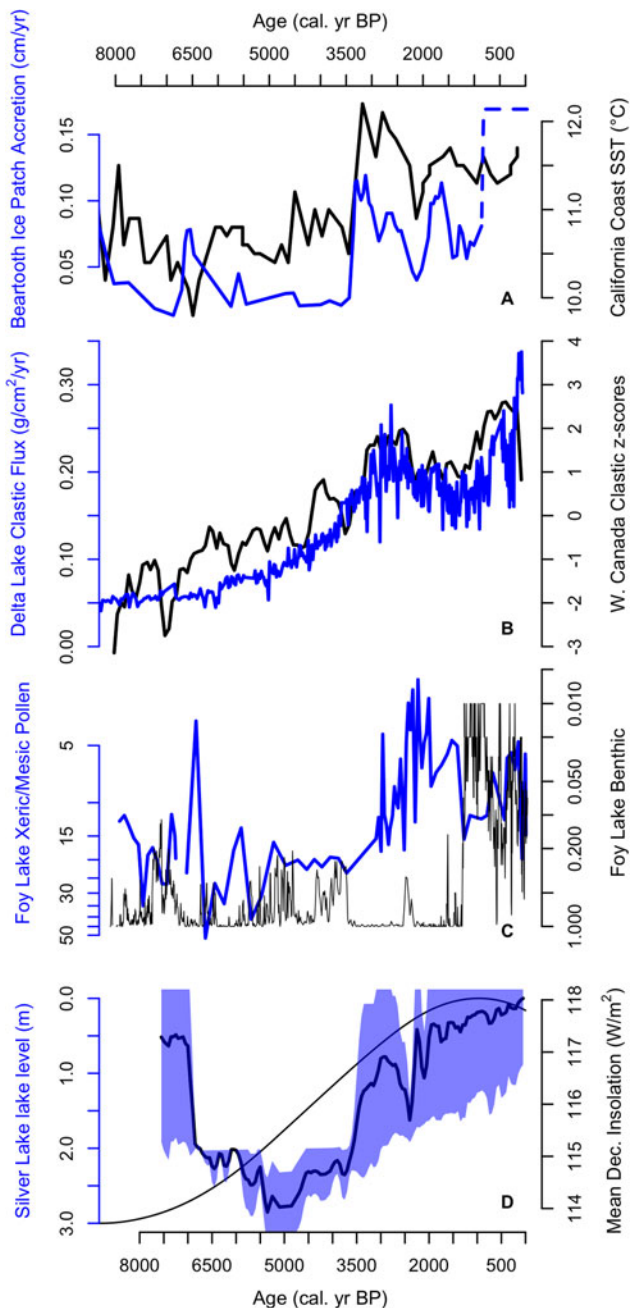
Figure 6. Plots showing different climate proxies versus age (cal yr BP): (A) Beartooth Ice Patch accretion rates from northern Wyoming showing increasing winter precipitation from mid- to late Holocene (blue line; Chellman et al., 2021) and an alkenone-based sea surface temperature (SST) reconstruction from off the coast of northern California showing increasing temperatures from the mid- to late Holocene (black line; Barron et al. 2003). (B) Average z-scores of the clastic content in lake sediment cores from Western Canada indicating glacial advances from mid- to late Holocene (black line; Menounos et al., 2009) and flux of clastic material into Delta Lake in the Teton Range in Wyoming, which is also used as a proxy for glacial advance (blue line; Larsen et al., 2020). (C) Plotted on inverted log scales are the ratio of xeric (*Pinus contorta, Pinus ponderosa, Pseudotsuga, Larix, Artemisia,* Poaceae, Chenopodiaceae, Cupressaceae) to mesic (Abies, Picea, *Tsuga heterophylla*) pollen taxa measured in a core from the middle of Foy Lake (blue line; Power et al., 2006, 2011), and % benthic diatoms from Foy Lake (black line; Stone and Fritz, 2006), indicating increasing moisture from mid- to late Holocene. (D) Our lake-level reconstruction from Silver Lake (blue line) shows a highstand from 7600 to 7000 cal yr BP, then a persistent lowstand from 7000 to 2800 cal yr BP, followed by a gradual increase to the modern highstand. Back line shows mean December insolation latitude of Silver Lake (47°N).

However, other data indicate opposite trends in northern Washington and southern British Columbia. At Castor and Lime lakes in northeast Washington, carbonate $\delta^{18}O$ exhibits long-term increases from the Mid- to Late Holocene, consistent with either reduced winter precipitation or increased evaporation since ca. 5000 cal yr BP (Fig. 7A; Nelson et al., 2011; Steinman et al., 2016, 2019; Routson et al., 2021). The Lime and Castor lakes $\delta^{18}O$ records differ from one another at centennial scales, and the variations must record different dynamics than those indicated by the Silver Lake sedimentary record. For example, Steinman et al. (2019) found high $\delta^{18}O$ values and inferred a 300-yr-long dry interval at Castor Lake in north-central Washington at ca. 7290 cal yr BP, after the eruption of Mt. Mazama, when the water levels at Silver, Foy, and Hidden lakes appear higher than during the Mid-Holocene (Fig. 7A; Shuman et al., 2009; Stone et al., 2019). Anderson et al. (2016) characterized Castor Lake as indicating potential evaporation, and Lime Lake as capturing the isotopic composition of precipitation received by the lake. Therefore, both $\delta^{18}O$ records could differ from the sedimentary evidence of lake-level changes dependent on net effective moisture. Furthermore, a $\delta^{18}O$ record from Jellybean Lake in Yukon Territory highlights potential effects from changes in atmospheric circulation processes during the Holocene (Anderson et al., 2016) that may also have affected the isotopic records at Castor and Lime lakes, and could amplify the differences in hydroclimate interpretations among records.

The wetter mid-Holocene inferred at Castor and Lime lakes is consistent with the interpretation of a diatom-based water-depth reconstruction from Felker Lake in British Columbia (Galloway et al., 2011). Galloway et al. (2011) inferred that the diatom-based water depths in the Mid-Holocene (6500–5000 cal yr BP) were greater than at present at Felker Lake. However, they did not consider that sediment infilling reduced the depth of Felker Lake by 9.5 m since the time of the Mazama Ash eruption. We adjusted the inferred water depth at Felker Lake by adding the elevation of the sediment-water interface to produce a record of the water-surface elevation comparable with our Silver Lake reconstruction. This revised reconstruction for Felker Lake indicates that the water-surface elevation of the lake was >4 m lower during the mid-Holocene than at present after accounting for the lower than modern sediment elevation at that time (Fig. 7B). A subsequent rise in the water levels of Felker Lake would be consistent with the histories of Silver and Foy lakes, and records of glacial advance and pollen-based paleoclimatic inferences from nearby sites in British Columbia (Menounos et al., 2009; Gavin et al., 2011), although the Felker Lake diatom record supports an earlier increase in water levels at ca. 6000 cal yr BP. Consistent with the overall rise in effective moisture in the revised Felker Lake reconstruction, Gavin et al. (2011) interpreted decreases in birch (*Betula*) coupled with increases in western hemlock (*T. heterophylla*) from the Mid- to Late Holocene at Eleanor Lake in British Columbia as indicative of increasing winter precipitation, suggesting a widespread shift to cooler, wetter conditions.

Climatic controls on the regional hydroclimatic changes

Overall, the long-term increases in precipitation in the Inland Northwest inferred from lake levels, glacial advances, ice-patch accretion, and paleobotanical records likely reflect orbitally forced changes in insolation. For example, Routson et al. (2019) pointed to the insolation-driven decrease in the latitudinal temperature
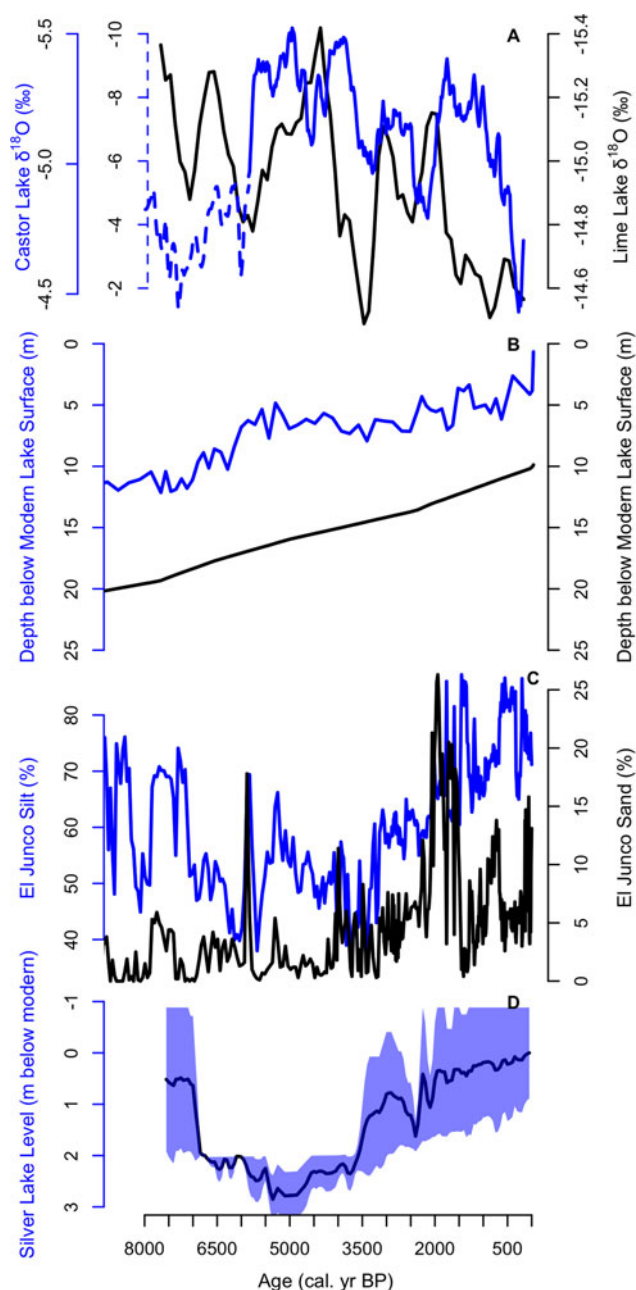
Figure 7. Plots showing different climate proxies versus age (cal yr BP): (A) δ^{18}O records from Castor Lake in north-central Washington (solid black line; Steinman et al., 2019; Nelson et al., 2011; dashed line is extended data from Routson et al., 2021) and Lime Lake in northeast Washington (blue line; Steinman et al., 2016) plotted as 400-yr moving averages, indicating decreasing winter precipitation or increasing evaporation from mid- to late Holocene. (B) Diatom-based lake-level reconstruction from Felker Lake in British Columbia plotted (blue line) after adjusting to account for the changing elevation of the sediment–water interface (black line; Galloway et al., 2011). (C) Black line shows % silt; blue line shows % sand from El Junco Lake in the Galápagos, indicating increasing El Niño–Southern Oscillation frequency from mid- to late Holocene (Conroy et al., 2008). (D) Silver Lake lake-level reconstruction with the line showing the median reconstructed lake level and the blue envelope representing the range of uncertainty (this study).

gradient between the equator and the Arctic to explain decreased precipitation in midlatitudes, including the Inland Northwest, during the Mid-Holocene. As Arctic summer insolation peaked at about 10 ka, followed by peak summer warmth at about 7 kyr, a reduced temperature gradient weakened midlatitude

westerly wind flow and cyclones, resulting in decreased midlatitude precipitation, including that associated with the flow of Pacific moisture into the Inland Northwest (Routson et al., 2019). Regionally, some climate models respond to mid-Holocene forcing by producing anticyclonic wind anomalies and upper-level ridging that reduce winter water-vapor transport from the central Pacific (Hermann et al., 2018). Increasing winter insolation throughout the Holocene may have favored atmospheric circulation and water vapor trends consistent with increased winter precipitation while declining summer insolation may have directly reduced evaporation, leading to the inferred hydrological change in the Inland Northwest (Whitlock et al., 2011; Liefert and Shuman, 2020).

Changes in atmospheric river events may have occurred within this synoptic framework of strengthening midlatitude westerly wind flow from the mid-Holocene to late Holocene, allowing atmospheric river events to either increase in frequency or intensity in western Montana from the mid- to late Holocene. Atmospheric river events, defined as long (>2000 km) and narrow (<1000 km) regions with an integrated water vapor content >20 mm play an important role in the present-day precipitation regime of western North America (Rutz et al., 2015). The greatest number of interior-penetrating atmospheric river events currently follows a trajectory from Oregon through Idaho into northwest Montana (Rutz et al., 2015). Along the Montana–Idaho border, ~35% of annual precipitation is related to atmospheric rivers (Gershunov et al., 2017), which would make the regional hydroclimate and the water-level histories of lakes potentially sensitive to changes in the frequency or intensity of these meteorological-scale events (Lora et al., 2017; Skinner et al., 2020). The frequency of such events and the amount of winter precipitation that they bring depend upon SST variations and the attendant pressure systems in the Pacific Ocean (Cayan, 1996; Dettinger et al., 1998; Gershunov et al., 2017; Kim et al., 2019). Diatom-inferred changes in storm frequencies may indicate changes in such events during the late-Holocene (Stone et al., 2016).

The modern hydrologic significance of atmospheric river events for western Montana may have been established during late Holocene (Rutz et al., 2014, 2015; Corringham et al., 2019), but simulations from Community Earth System Model version 1.2 (CESM1.2) by Skinner et al. (2020) indicated decreasing, not increasing, atmospheric river precipitation from the mid- to late Holocene in the Pacific Northwest. The CESM1.2 produces a drier mid-Holocene relative to pre-Industrial conditions in most of the United States, and a simulated northward shift in the location of the majority of atmospheric rivers in the Mid-Holocene that reduced precipitation in the region centered around 50°N (Skinner et al., 2020). The decreasing atmospheric river activity from the mid- to late Holocene in the Pacific Northwest, particularly in winter (Skinner et al., 2020), could explain why the records from Lime Lake and Castor Lake in northern Washington show a wet Mid-Holocene relative to the late Holocene, in contrast to the hydrologic changes at the more southerly Silver Lake location (Steinman et al., 2016, 2019). However, the simulations are not consistent with the corrected sediment accumulation lake-level record from Felker Lake (Fig. 7B) or the paleobotanical record from British Columbia (Gavin et al., 2011), both of which indicate broad-scale increases in precipitation from the Mid- to Late Holocene.

An apparent correlation between an alkenone-based SST record from coastal California and the Silver Lake lake-level reconstruction (Fig. 6) is sufficiently strong (R=−0.62 based on interpolating both series to common 100-yr time steps;

Supplementary Figure S1) to warrant further examination into the relationship between North Pacific SSTs and Inland Northwest precipitation. The alkenone-based SST reconstruction (Barron et al., 2003) shows similar trends and patterns to the lake-level reconstruction from Silver Lake (Fig. 6A) and ice-patch accumulation and glacial-advance records in northwest Wyoming (Fig. 6; Larsen et al., 2020; Chellman et al., 2021). Some climate simulations favor anticyclonic wind anomalies over the California margin in the mid-Holocene, which may have favored upwelling, low SSTs, and reduced inland moisture transport as compared to present-day conditions in a manner that could explain the relationship (Hermann et al., 2018). Likewise, in the historical record (AD 1948 to 2017), increased North Pacific SSTs have coincided with increased vapor transport to western North America (Gershunov et al., 2017) and North American Regional Reanalysis data (Kalnay et al., 1996) indicate that annual precipitation declines over the western United States during years with low SSTs off the coast of California. If higher SSTs in the northeastern Pacific are responsible for more winter precipitation in the interior Northwest, however, it would conflict with evidence of decreased snowpack in the northern Rockies coinciding with high SSTs in the northeastern Pacific Ocean and the associated strengthening of the Aleutian Low that has occurred in the last 30 years (Pederson et al., 2011a).

The increase in Silver Lake water level during the late Holocene may also indicate a possible change in the frequency or strength of El Niño events, but historic precipitation north of the American Southwest is not significantly correlated with El Niño–Southern Oscillation indices (Shinker and Bartlein, 2009; McAfee and Wise, 2016; Heyer et al., 2017). Although the frequency and intensity of El Niño is inferred to have increased from the Mid- to Late Holocene (Fig. 7C; Moy et al., 2002; Conroy et al., 2008), any direct relationship with the Silver Lake record (Fig. 7D), with or without attendant atmospheric river dynamics, is unclear.

Regardless of the cause, the rise in lake levels, such as seen in records from Silver, Foy, and Hidden lakes, may indicate an eastward expansion of the high precipitation regimes typical of the Pacific Northwest into northwest Montana (Fig. 1B). However, the uncertainty in definitively attributing the Mid- to Late-Holocene increase in precipitation in the Inland Northwest to a proximate cause requires further investigation of the Holocene relationships among different regions and among different types of proxy records, such as those generated from stable isotopes, pollen, tree rings, and lake levels.

CONCLUSIONS

Our lake-level reconstruction from Silver Lake indicates an increasing moisture trend in northwestern Montana over the past 7600 years. The lake-level record includes evidence of multi-century hydrologic fluctuations, such as a phase of high water from 7600–7000 cal yr BP. Sand layers and an associated sedimentary unconformity across the lake's shallow bay document the major feature of the record, which is a substantial reduction in water levels from 7000–2800 cal yr BP, consistent with other regional records such as Foy Lake (Shuman et al., 2009). The rise in water levels after ca. 2800 cal yr BP may be attributed to various factors such as a decreasing latitudinal temperature gradient, and effects on atmospheric circulation, including the frequency or intensity or atmospheric river vapor transport. Regardless of the causes, the substantial hydrologic change seen in the record at Silver Lake likely had important ecological and environmental consequences.

REFERENCES

Anderson, L., Berkelhammer, M., Barron, J.A., Steinman, B.A., Finney, B.P., Abbott, M.B., 2016. Lake oxygen isotopes as recorders of North American Rocky Mountain hydroclimate: Holocene patterns and variability at multi-decadal to millennial time scales. *Global and Planetary Change* **137**, 131–148.

Barron, J.A., Anderson, L., 2011. Enhanced Late Holocene ENSO/PDO expression along the margins of the eastern North Pacific. *Quaternary International* **235**, 3–12.

Barron, J.A., Heusser, L., Herbert, T., Lyle, M., 2003. High-resolution climatic evolution of coastal northern California during the past 16,000 years. *Paleoceanography and Paleoclimatology* **18**, 1020. https://doi.org/10.1029/2002PA000768.

Bartlein, P.J., Anderson, K.H., Anderson, P.M., Edwards, M.E., Mock, C.J., Thompson, R.S., Webb, R.S., Webb III, T., Whitlock, C., 1998. Paleoclimate simulations for North America over the past 21,000 years: features of the simulated climate and comparisons with paleoenvironmental data. *Quaternary Science Reviews* **17**, 549–585.

Bracht-Flyr, B., Fritz, S.C., 2012. Synchronous climatic change inferred from diatom records in four western Montana lakes in the U.S. Rocky Mountains. *Quaternary Research* **77**, 456–467.

Brunelle, A., Rehfeldt, G.E., Bentz, B., Munson, A.S., 2008. Holocene records of *Dendroctonus* bark beetles in high elevation pine forests of Idaho and Montana, USA. *Forest Ecology and Management* **255**, 836–846.

Brunelle, A., Whitlock, C., Bartlein, P., Kipfmueller, K., 2005. Holocene fire and vegetation along environmental gradients in the Northern Rocky Mountains. *Quaternary Science Reviews* **24**, 2281–2300.

Cayan, D.R., 1996. Interannual climate variability and snowpack in the western United States. *Journal of Climate* **9**, 928–948.

Chellman, N.J., Pederson, G.T., Lee, C.M., McWethy, D.B., Puseman, K., Stone, J.R., Brown, S.R., McConnell, J.R., 2021. High elevation ice patch documents Holocene climate variability in the northern Rocky Mountains. *Quaternary Science Advances* **3**, 100021. https://doi.org/10.1016/j.qsa.2020.100021.

Conroy, J.L., Overpeck, J.T., Cole, J.E., Shanahan, T.M., Steinitz-Kannan, M., 2008. Holocene changes in eastern tropical Pacific climate inferred from a Galápagos lake sediment record. *Quaternary Science Reviews* **27**, 1166–1180.

Corringham, T.W., Ralph, F.M., Gershunov, A., Cayan, D.R., Talbot, C.A., 2019. Atmospheric rivers drive flood damages in the western United States. *Science Advances* **5**, eaax4631. https://doi.org/10.1126/sciadv.aax4631.

Dettinger, M.D., Cayan, D.R., Diaz, H.F., Meko, D.M., 1998. North–South precipitation patterns in western North America on interannual-to-decadal timescales. *Journal of Climate* **11**, 3095–3111.

Diffenbaugh, N.S., Ashfaq, M., Shuman, B., Williams, J.W., Bartlein, P.J., 2006. Summer aridity in the United States: Response to mid-Holocene changes in insolation and sea surface temperature. *Geophysical Research Letters* **33**, L22712. https://doi.org/10.1029/2006GL028012.

Digerfeldt, G., 1986. Studies on past lake-level fluctuations. In: Berglund, B.E. (Ed.), 1986. *Handbook of Holocene Palaeoecology and Palaeohydrology*. Wiley, Chichester, pp. 127–143.

Galloway, J.M., Lenny, A.M., Cumming, B.F., 2011. Hydrological change in the central interior of British Columbia, Canada: diatom and pollen evidence of millennial-to-centennial scale change over the Holocene. *Journal of Paleolimnology* **45**, 183–197.

Gavin, D.G., 2009. The coastal-disjunct mesic flora in the inland Pacific Northwest of USA and Canada: refugia, dispersal and disequilibrium. *Diversity and Distributions* **15**, 972–982.

Gavin, D.G., Henderson, A.C.G., Westover, K.S., Fritz, S.C., Walker, I.R., Leng, M.J., Hu, F.S., 2011. Abrupt Holocene climate change and potential response to solar forcing in western Canada. *Quaternary Science Reviews* **30**, 1243–1255.

Gershunov, A., Shulgina, T., Ralph, F.M., Lavers, D.A., Rutz, J.J., 2017. Assessing the climate-scale variability of atmospheric rivers affecting western North America. *Geophysical Research Letters* **44**, 7900–7908.

Harrison, S.P., Digerfeldt, G., 1993. European lakes as palaeohydrological and palaeoclimatic indicators. *Quaternary Science Reviews* **12**, 233–248.

Hermann, N.W., Oster, J.L., Ibarra, D.E., 2018. Spatial patterns and driving mechanisms of mid-Holocene hydroclimate in western North America. *Journal of Quaternary Science* **33**, 421–434.

Herring, E.M., Gavin, D.G., 2015. Climate and vegetation since the Last Interglacial (MIS 5e) in a putative glacial refugium, northern Idaho, USA. *Quaternary Science Reviews* **117**, 82–95.

Herring, E.M., Gavin, D.G., Dobrowski, S.Z., Fernandez, M., Hu, F.S., 2017. Ecological history of a long-lived conifer in a disjunct population. *Journal of Ecology* **106**, 319–332.

Heyer, J.P., Brewer, S.C., Shinker, J.J., 2017. Using high-resolution reanalysis data to explore localized western North America hydroclimate relationships with ENSO. *Journal of Climatology* **30**, 5395–5417.

Hijmans, R.J., van Etten, J., Sumner, M., Cheng, J., Baston, D., Bevan, A., Bivand, R., Busetto, L., Canty, M., Fasoli, B., Forrest, D., 2022. *raster: Geographic Data Analysis and Modeling.* v. 3.4-5. https://CRAN.R-project.org/package=raster.

Kalnay, E., Kanamitsu, M., Kistler, R., Collins, W., Deaven, D., Gandin, L., Iredell, M., *et al*. 1996. The NCEP/NCAR 40-year reanalysis project. *Bulletin of the American Meteorological Society* **77**, 437–472.

Kim, H.-M., Zhou, Y., Alexander, M.A., 2019. Changes in atmospheric rivers and moisture transport over the Northeast Pacific and western North America in response to ENSO diversity. *Climate Dynamics* **52**, 7375–7388.

Krimmel, R.M., 2002. Glaciers of the coterminous United States. In: Williams, R.S., Ferrigno, J.G. (Eds.), Satellite Images of Glaciers of the World: North America (excluding Alaska) *U.S. Geological Survey Professional Paper* 1386-J, 1–56.

Kutzbach, J., Gallimore, R., Harrison, S., Behling, P., Selin, R., Laarif, F., 1998. Climate and biome simulations for the past 21,000 years. *Quaternary Science Reviews* **17**, 473–506.

Larsen, D.J., Crump, S.E., Blumm, A., 2020. Alpine glacier resilience and Neoglacial fluctuations linked to Holocene snowfall trends in the western United States. *Science Advances* **6**, eabc7661. https://doi.org/10.1126/sciadv.abc7661.

Liefert, D.T., Shuman, B.N., 2020. Pervasive desiccation of North American lakes during the Late Quaternary. *Geophysical Research Letters* **47**, e2019GL086412. https://doi.org/10.1029/2019GL086412.

Livneh, B., Rosenberg, E.A., Lin, C., Nijssen, B., Mishra, V., Andreadis, K.M., Maurer, E.P., Lettenmaier, D.P., 2013. A long-term hydrologically based dataset of land surface fluxes and states for the conterminous United States: update and extensions. *Journal of Climate* **26**, 9384–9392.

Locke, W.W., 1990. Late Pleistocene glaciers and the climate of western Montana, U.S.A. *Arctic and Alpine Research* **22**, 1–13.

Lonn, J.D., McFaddan, M.D., 1999. *Geologic Map of the Montana Part of the Wallace 30′ × 60′ Quadrangle, Western Montana. 1;100,000.* Montana Bureau of Mines and Geology Open File 388. Montana Bureau of Mines and Geology, Butte.

Lora, J.M., Mitchell, J.L., Risi, C., Tripati, A.E., 2017. North Pacific atmospheric rivers and their influence on western North America at the Last Glacial Maximum. *Geophysical Research Letters* **44**, 1051–1059.

McAfee, S.A., Wise, E.K., 2016. Intra-seasonal and inter-decadal variability in ENSO impacts on the Pacific Northwest. *International Journal of Climatology* **36**, 508–516.

Menounos, B., Osborn, G., Clague, J.J., Luckman, B.H., 2009. Latest Pleistocene and Holocene glacier fluctuations in western Canada. *Quaternary Science Reviews* **28**, 2049–2074.

Moy, C.M., Seltzer, G.O., Rodbell, D.T., Anderson, D.M., 2002. Variability of El Niño/Southern Oscillation activity at millennial timescales during the Holocene epoch. *Nature* **420**, 162–165.

Nelson, D.B., Abbott, M.B., Steinman, B., Polissar, P.J., Stansell, N.D., Ortiz, J.D., Rosenmeier, M.F., Finney, B.P., Riedel, J., 2011. Drought variability in the Pacific Northwest from a 6,000-yr lake sediment record. *Proceedings of the National Academy of Sciences of the United States of America* **108**, 3870–3875.

Newby, P.E., Shuman, B.N., Donnelly, J.P., Karnauskas, K.B., Marsicek, J., 2014. Centennial-to-millennial hydrologic trends and variability along the North Atlantic Coast, USA, during the Holocene. *Geophysical Research Letters* **41**, 4300–4307.

Parnell, A., McJames, N., Wundervald, B., Murphy, K., Maia M., Shoari Nejad, A.S., Goh, Y.C., 2021. *Bchron: radiocarbon dating, age-depth modelling, relative sea level rate estimation, and non-parametric phase modelling, v. 4.7.6.* https://CRAN.R-project.org/package=Bchron.

Pederson, G.T., Gray, S.T., Ault, T., Marsh, W., Fagre, D.B., Bunn, A.G., Woodhouse, C.A., Graumlich, L.J., 2011a. Climatic controls on the snowmelt hydrology of the Northern Rocky Mountains. *Journal of Climate* **24**, 1666–1687.

Pederson, G.T., Gray, S.T., Woodhouse, C.A., Betancourt, J.L., Fagre, D.B., Littell, J.S., Watson, E., Luckman, B.H., Graumlich, L.J., 2011b. The unusual nature of recent snowpack declines in the North American Cordillera. *Science* **333**, 332–335.

Power, M.J., Whitlock, C., Bartlein, P.J., 2011. Postglacial fire, vegetation, and climate history across an elevational gradient in the Northern Rocky Mountains, USA and Canada. *Quaternary Science Reviews* **30**, 2520–2533.

Power, M.J., Whitlock, C., Bartlein, P., Stevens, L.R., 2006. Fire and vegetation history during the last 3800 years in northwestern Montana. *Geomorphology* **75**, 420–436.

Pribyl, P., Shuman, B.N., 2014. A computational approach to Quaternary lake-level reconstruction applied in the central Rocky Mountains, Wyoming, USA. *Quaternary Research* **82**, 249–259.

PRISM Climate Group, 2021. Oregon State University. https://prism.oregonstate.edu. [accessed January 18, 2021]

Reimer, P.J., Austin, W.E.N., Bard, E., Bayliss, A., Blackwell, P.G., Bronk Ramsey, C., Butzin, M., *et al*., 2020. The IntCal20 Northern Hemisphere radiocarbon age calibration curve (0–55 cal kBP). *Radiocarbon* **62**, 725–757.

Routson, C.C., Kaufman, D.S., McKay, N.P., Erb, M.P., Arcusa, S.H., Brown, K.J., Kirby, M.E., *et al*., 2021. A multiproxy database of western North American Holocene paleoclimate records. *Earth System Science Data* **13**, 1614–1632.

Routson, C.C., McKay, N.P., Kaufman, D.S., Erb, M.P., Goosse, H., Shuman, B.N., Rodysill, J.R., Ault, T., 2019. Mid-latitude net precipitation decreased with Arctic warming during the Holocene. *Nature* **568**, 83–87.

Rowan, D.J., Kalff, J., Rasmussen, J.B., 1992. Estimating the mud deposition boundary depth in lakes from wave theory. *Canadian Journal of Fisheries and Aquatic Sciences* **49**, 2490–2497.

Rutz, J.J., Steenburgh, W.J., Ralph, F.M., 2014. Climatological characteristics of atmospheric rivers and their inland penetration over the western United States. *Monthly Weather Review* **142**, 905–921.

Rutz, J.J., Steenburgh, W.J., Ralph, F.M., 2015. The inland penetration of atmospheric rivers over western North America: A Lagrangian analysis. *Monthly Weather Review* **143**, 1924–1944.

Schoenemann, S.W., Martin, J.T., Pederson, G.T., McWethy, D.B., 2020. 2,200-year tree-ring and lake-sediment based snowpack reconstruction for the northern Rocky Mountains highlights the historic magnitude of recent snow drought. *Quaternary Science Advances* **2**, 100013. https://doi.org/10.1016/j.qsa.2020.100013.

Schweger, C.E., Hickman, M., 1989. Holocene paleohydrology of central Alberta: testing the general-circulation-model climate simulations. *Canadian Journal of Earth Sciences* **26**, 1826–1833. h

Shapley, M.D., Ito, E., Donovan, J.J., 2009. Lateglacial and Holocene hydroclimate inferred from a groundwater flow-through lake, Northern Rocky Mountains, USA. *The Holocene* **19**, 523–535.

Shinker, J.J., Bartlein, P.J., 2009. Visualizing the large-scale patterns of ENSO-related climate anomalies in North America. *Earth Interactions* **13**, 1–50.

Shinker, J.J., Bartlein, P.J., 2010. Spatial variations of effective moisture in the western United States. *Geophysical Research Letters* **37**, L02701. https://doi.org/10.1029/2009GL041387.

Shuman, B., 2003. Controls on loss-on-ignition variation in cores from two shallow lakes in the northeastern United States. *Journal of Paleolimnology* **30**, 371–385.

Shuman, B., Henderson, A.K., Colman, S.M., Stone, J.R., Fritz, S.C., Stevens, L.R., Power, M.J., Whitlock, C., 2009. Holocene lake-level trends in the Rocky Mountains, U.S.A. *Quaternary Science Reviews* **28**, 1861–1879.

Shuman, B.N., Pribyl, P., Buettner, J., 2015. Hydrologic changes in Colorado during the mid-Holocene and Younger Dryas. *Quaternary Research* **84**, 187–199.

Shuman, B.N., Serravezza, M., 2017. Patterns of hydroclimatic change in the Rocky Mountains and surrounding regions since the last glacial maximum. *Quaternary Science Reviews* **173**, 58–77.

Skinner, C.B., Lora, J.M., Payne, A.E., Poulsen, C.J., 2020. Atmospheric river changes shaped mid-latitude hydroclimate since the mid-Holocene. *Earth and Planetary Science Letters* **541**, 116293. https://doi.org/10.1016/j.epsl.2020.116293.

Steinman, B.A., Nelson, D.B., Abbott, M.B., Stansell, N.D., Finkenbinder, M.S., Finney, B.P., 2019. Lake sediment records of Holocene hydroclimate and impacts of the Mount Mazama eruption, north-central Washington, USA. *Quaternary Science Reviews* **204**, 17–36.

Steinman, B.A., Pompeani, D.P., Abbott, M.B., Ortiz, J.D., Stansell, N.D., Finkenbinder, M.S., Mihindukulasooriya, L.N., Hillman, A.L., 2016. Oxygen isotope records of Holocene climate variability in the Pacific Northwest. *Quaternary Science Reviews* **142**, 40–60.

Stevens, L.R., Stone, J.R., Campbell, J., Fritz, S.C., 2006. A 2200-yr record of hydrologic variability from Foy Lake, Montana, USA, inferred from diatom and geochemical data. *Quaternary Research* **65**, 264–274.

Stone, J.R., Fritz, S.C., 2004. Three-dimensional modeling of lacustrine diatom habitat areas: Improving paleolimnological interpretation of planktic : benthic ratios. *Limnology and Oceanography* **49**, 1540–1548.

Stone, J.R., Fritz, S.C., 2006. Multidecadal drought and Holocene climate instability in the Rocky Mountains. *Geology* **34**, 409–412.

Stone, J.R., Saros, J.E., Pederson, G.T., 2016. Coherent late-Holocene climate-driven shifts in the structure of three Rocky Mountain lakes. *The Holocene* **26**, 1103–1111.

Stone, J.R., Saros, J.E., Spanbauer, T.L., 2019. The influence of fetch on the Holocene thermal structure of Hidden Lake, Glacier National Park. *Frontiers in Earth Science* **7**. https://doi.org/10.3389/feart.2019.00028.

USGS (U.S. Geological Survey), 2017. 1/3rd arc-second Digital Elevation Models (DEMs) - USGS National Map 3DEP Downloadable Data Collection. U.S. Geological Survey. https://www.usgs.gov/3d-elevation-program. [accessed March 5, 2022]

Whitlock, C., Bartlein, P.J., 1993. Spatial variations of Holocene climatic change in the Yellowstone region. *Quaternary Research* **39**, 231–238.

Whitlock, C., Briles, C.E., Fernandez, M.C., Gage, J., 2011. Holocene vegetation, fire and climate history of the Sawtooth Range, central Idaho, USA. *Quaternary Research* **75**, 114–124.

Whitlock, C., Marlon, J., Briles, C., Brunelle, A., Long, C., Bartlein, P., 2008. Long-term relations among fire, fuel, and climate in the northwestern US based on lake-sediment studies. *International Journal of Wildland Fire* **17**, 72–83.